

A MEASUREMENT OF THE ANGULAR POWER SPECTRUM OF THE MICROWAVE BACKGROUND MADE FROM THE HIGH CHILEAN ANDES

E. TORBET¹, M. J. DEVLIN², W. B. DORWART¹, T. HERBIG¹, A. D. MILLER¹, M. R. NOLTA¹, L. PAGE¹, J. PUCHALLA², H. T. TRAN¹

Submitted to ApJL 1999 April 30; revised 1999 June 10

ABSTRACT

We report on a measurement of the angular spectrum of the anisotropy of the microwave sky at 30 and 40 GHz between $l = 50$ and $l = 200$. The data, covering roughly 600 deg^2 , support a rise in the angular spectrum to a maximum with $\delta T_l \approx 85 \mu\text{K}$ at $l = 200$. We also give a 2-sigma upper limit of $\delta T_l < 122 \mu\text{K}$ at $l = 432$ at 144 GHz. These results come from the first campaign of the Mobile Anisotropy Telescope (MAT) on Cerro Toco, Chile. To assist in assessing the site, we present plots of the fluctuations in atmospheric emission at 30 and 144 GHz.

Subject headings: cosmic microwave background — cosmology: observations — atmospheric effects

1. INTRODUCTION

The characterization of the CMB anisotropy is essential for understanding the process of cosmic structure formation (e.g. Hu et al. 1997). If some of the currently popular models prove correct, the anisotropy may be used to strongly constrain cosmological parameters (Jungman et al. 1995, Bond et al. 1998). Here we report the results from the *TOCO97* campaign of the Mobile Anisotropy Telescope (MAT) experiment.

2. INSTRUMENT

The MAT telescope is comprised of the QMAP balloon gondola and instrument (Devlin et al. 1998), mounted on the azimuthal bearing of a surplus Nike Ajax military radar trailer³. The receiver has five cooled corrugated feed horns, one at K_a band (31 GHz), two at Q band (42 GHz), and two at D band (144 GHz). Each of the K_a and Q band horns feed two HEMT-based (high electron mobility transistor) amplifiers (Pospieszalski 1992) with one in each polarization. The two D band horns each feed a single SIS detector (Kerr et al. 1993) with one horn in each polarization. This gives a total of eight radiometry channels in the experiment⁴. A Sumitomo mechanical refrigerator cools the HEMT amplifiers to 35 K and the SIS receivers to 4 K.

The telescope optics are similar to those used for three ground-based observing campaigns in Saskatoon, SK (Wollack et al. 1997, *SK*). The feeds underilluminate an ambient temperature 0.85 m off-axis parabolic reflector which in turn underilluminates a computer controlled 1.8 m \times 1.2 m resonant chopping flat mirror. The beams are scanned horizontally across the sky in a ≈ 4.6 Hz sinusoidal pattern. The outputs of the detectors are AC coupled at 0.15 Hz and sampled N_c times during each chopper cycle ($N_c = 80$ for K_a and Q bands, and $N_c = 320$ for

D band). The telescope is inside an aluminum ground screen which is fixed with respect to the receiver and parabola.

The telescope pointing (Table 1) is established through observations of Jupiter and is monitored with two redundant encoders on both the azimuth bearing and on the chopper. The absolute errors in azimuth and elevation are $0^\circ 04$, and the relative errors are $< 0^\circ 01$. The chopper position is sampled 80 times per chop. When its *rms* position over one cycle deviates by more than $0^\circ 015$ from the average position (due to wind, etc.), we reject the data.

Table 1. TOCO97 beam characteristics

Feed	Az deg	El deg	Ω_{meas} 10^{-4} sr	θ_{avg}^{FWHM} deg
$K_a1/2$	203.13	41.75	2.75	0.90
$Q1/2$	206.75	41.85	1.69	0.70
$Q3/4$	206.70	39.25	1.77	0.72
$D1$	205.00	40.44	0.183	0.23

3. OBSERVATIONS AND CALIBRATION

Data were taken at a 5200 m site⁵ on the side of Cerro Toco (lat. = $-22^\circ 95'$ long. = $67^\circ 775'$), near San Pedro de Atacama, Chile, from Oct. 20, 1997 to Dec 15, 1997. The receiver was operational 90% of the available time. For the anisotropy data, the primary optical axis is fixed at $az = 204^\circ 9'$, $el = 40^\circ 5'$, $\delta = -62^\circ 6'$ and the chopper scans with an azimuthal amplitude of $2^\circ 96'$ ($8^\circ 93'$ on the sky) as the sky rotates through the beam. The telescope position was not wobbled to the other side of the South Celestial Pole as for the *SK* measurements in the North. The *rms* outputs of the K_a2 and $D1$ channels are shown in Fig. 1.

¹Princeton University, Physics Department, Jadwin Hall, Princeton, NJ 08544

²University of Pennsylvania, Department of Physics and Astronomy, David Rittenhouse Laboratory, Philadelphia, PA 19104

³Details of the experiment, synthesis vectors, data, and analysis code may be found at <http://www.hep.upenn.edu/CBR/> and <http://pupgg.princeton.edu/~cmb>

⁴HEMT amplifiers have improved considerably since this time (Pospieszalski et al. 1997) and SIS receivers are generally more sensitive than what we achieved. In 1997, one of the D channels and one of the Q channels did not have sufficient sensitivity to warrant a full analysis.

⁵The Cerro Toco site of the Universidad Catolica de Chile was made available through the generosity of Prof. Hernán Quintana, Dept. of Astronomy and Astrophysics. It is near the proposed MMA site.

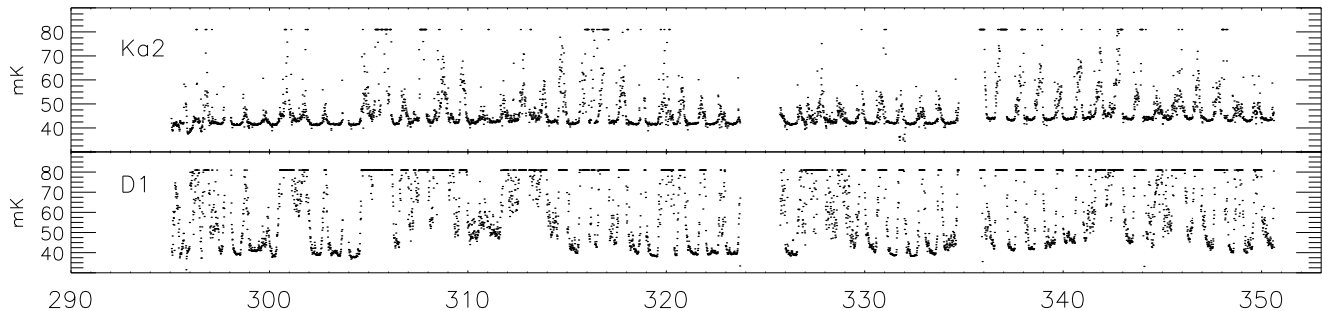


FIG. 1.— The *rms* detector output in antenna temperature of the K_a2 and $D1$ channels averaged over 0.68 ms (with the chopper running at the nominal amplitude) vs. day of year in 1997. The sky is most stable between 10 PM and 10 AM local time. Similar results from 1998 are consistent with the NRAO opacity measurements (<http://www.tuc.nrao.edu/mma/sites/sites.html>).

Jupiter is used to calibrate all channels and map the beams. Its brightness temperature is 152, 160, 170 K for K_a through D bands respectively (Griffin et al. 1986, Ulich et al. 1981), with an intrinsic calibration error of $\approx 5\%$. We account for the variation in angular diameter. We also observe Jupiter with multiple relative azimuthal offsets to verify the chopper calibration.

The uncertainty in the beam solid angle for the K_a and Q bands is $\approx 5\%$ as determined from the standard deviation of beam measurements for the *MAT* and *QMAP* experiments. From a global fit of the clear-weather Jupiter calibrations, the standard deviation in the fitted amplitudes is 6%. These sources of calibration error dominate the error from the uncertainty in the passband. The total 1σ calibration error is obtained by combining the intrinsic, beam, and measurement errors in quadrature resulting in 10%, 10%, and 11% in K_a through D respectively.

A thermally-stabilized noise source at $T_{\text{eff}} \approx 1$ K is switched on twice for 40 msec every 100 seconds as a relative calibration. The pulse height is correlated to the Jupiter calibrations in the K_a and Q channels. The variation in detector gain corrected for with these calibration pulses is roughly 5%. No such correction was made for D band.

4. DATA REDUCTION

The reduction is similar to that of the SK experiment (Netterfield et al. 1997). The raw data, d_i , are multiplied by “n-pt” synthesis vectors, $SV_{n,i}$ (where i ranges from 1 to N_c) to yield the effective temperature corresponding to a multilobed beam on the sky, $H(\Omega)$. For example, we refer to the classic three-lobed beam produced by a “double difference” as the “3-pt harmonic” and write $t_3 = \sum_{i=1}^{N_c} SV_{3,i} d_i$. We also generate the quadrature signal q_n (data with chopper sweeping in one direction minus that with the sweeping in the other direction) and fast-dither signal f_n^d (one value of t_n minus the subsequent one). For both $K_a1/2$ and $Q3/4$ we analyze the unpolarized weighted mean of the combined detector outputs.

The phase of the data relative to the beam position is determined with both Jupiter and observations of the galaxy. We know we are properly phased when the quadrature signal from the galaxy is zero for all harmonics.

The harmonics are binned according to the right ascension at the center of the chopper sweep. The number of bins depends on the band and harmonic (Table 2). For

each night, we compute the mean and variance of all the t_n , q_n , and f_n^d corresponding to a bin. These numbers are appropriately averaged over the campaign and used in the likelihood analysis.

From the raw dataset of 814250 5s averages, we filter out time spent on instrument calibration (6%), celestial calibrations (11%), observations of the galaxy & daytime (53%), and bad pointing (4%). Accounting for overlap, these cut a total of 57%. The data span $RA = 0^\circ$ to 140° ($b = -55^\circ$ to -10°).

The data are selected according to the weather by examining each harmonic independently. We first flag 5s averages with a large *rms*. The unflagged data are divided up into 15 minute sections and the *rms* of the t_n found. For 15 m sections with *rms* $> 2\sigma$, the constituent 5s averages are not used, as well as those of the preceding and succeeding 15 m sections. We ensure that the cut does not bias the statistical weight. As a final cut, nights with less than 4.7 hours of data are excluded. Repeating the analysis with increased cut values produces statistically similar (within 1σ) results. The atmosphere cut selects roughly the same sections for K_a and Q . In the analyses, we discard the 2 and 3-pt data as it is corrupted by atmospheric fluctuations and variable instrumental offsets. If the 4-pt is corrupted, it is at the 1σ level and not readily detectable.

The stability of the instrument is assessed through internal consistency checks and with the distribution of the offset of each harmonic. The offset is the average of a night of data after the cuts have been applied (ranges from 5-10 hours) and is of magnitude $\approx 200 \mu\text{K}$ with error $20 \mu\text{K}$. In general, the offset remains constant for a few nights and then jumps 3-5 sigma. The resulting χ^2/ν is typically between 4 and 20 for the data over the full campaign and is ≈ 1 for the quadrature signal. In general, a change in offset can have any time scale. The q_n and f_n^d are sensitive to $\tau = 0.25$ s. We also monitor a slow dither (difference of the subsequent 5 sec averages) with $\tau = 5$ s and a night-to-night dither with $\tau = 24$ h. For the final analysis, we delete one seven day section that has a large jump in offset. To eliminate the potential effect of slow variations in offset, we remove the slope and mean for each night. This is accounted for in the quoted result (both the constraint matrix method, Bond et al. 1998b, and marginalization, Bond et al. 1991 give similar corrections) and does not significantly alter the results over the subtraction of a simple mean. As a test, we have also tried removing quadratic

and cubic terms from the offset, with no significant changes in the answer. In summary, there is no evidence that the small instability in the offset affects our results.

We examined the variations in the power spectrum of the synchronously co-added raw HEMT data, and found no evidence for microphonics. However, a microphonic coupling to the SIS detector was exacerbated after situating the telescope at the site. After filtering, residual signals persisted in the quadrature channels (though not in the fast and slow dithers) and so we report only 95% upper limits for the D channel, specifically $\delta T_l < 180 \mu\text{K}$ at $\ell = 325$ and $\delta T_l < 122 \mu\text{K}$ at $\ell = 432$.

The primary effect of data editing is to increase the error bar per point and decrease the upper limits of the null tests. Of the 169 null tests (Table 2 plus fast, slow, and night dithers), there are only three failures. The distribution of the reduced χ^2 of the null tests is consistent with noise and inconsistent with any signal. When the data are combined into groups of harmonics and bands, all null tests are consistent with noise.

5. ANALYSIS AND DISCUSSION

The analysis of the individual harmonics, because the windows are so narrow, essentially corresponds to finding $\delta T_l' = \sqrt{(\Delta_{tot}^2 - \Delta_{inst}^2)/I(W)}$, where Δ_{tot}^2 is the variance of the data for each harmonic, Δ_{inst}^2 is the variance due to atmospheric and instrumental noise, and $I(W) = \sum W_l/l$. W_l is the window function, as defined in Bond 1996. The full likelihood analysis provides a formal way of determining δT_l that includes correlations and gives the correct error bar in the low signal-to-noise limit.

The error in $I(W)$ is determined from the scatter in the beam values. We find $\delta I(W)/I(W) \lesssim 0.01$ for all bands and harmonics. The mean variance, Δ_{inst}^2 , is determined directly from the uncertainties in each bin. If these uncertainties are somehow biased, the results of the simple test and full likelihood will be biased. We examine the distribution of all the data for each harmonic from all the nights after removing the mean value of each sky bin. The width of this distribution agrees with the mean error bar indicating that the error per point is not biased. Also, the ratio of the error bars between harmonics agrees with the analytic calculation.

In the full analysis (Fig. 2), we include all known correlations inherent in the observing strategy. From the data, we determine the correlations between harmonics due to the atmosphere, detector noise, and non-orthogonality of the synthesis vectors. The correlation coefficients between bands due to the atmosphere are of order 0.05. We also examine the autocorrelation function of the data for a single harmonic to ensure that atmospheric fluctuations do not correlate one bin to the next. The quoted results are insensitive to the precise values of the off-diagonal terms

of the covariance matrix.

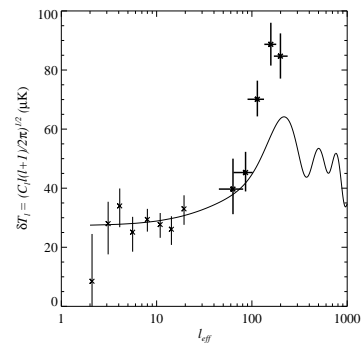


FIG. 2.— Combined analysis of data in Table 2. The values are $(l, \delta T_l [\mu\text{K}]) = (63^{+18}_{-18}, 40^{+10}_{-9}), (86^{+16}_{-22}, 45^{+7}_{-6}), (114^{+20}_{-24}, 70^{+6}_{-6}), (158^{+22}_{-23}, 89^{+7}_{-7}), (199^{+38}_{-29}, 85^{+8}_{-8})$. Error bars are “1 σ statistical”; calibration error is not included. The COBE/DMR points are from Tegmark 1997. The solid curve is standard CDM ($\Omega_b = 0.05$, $h = 0.5$).

These results are similar to previous results obtained with this technique (SK) though the experiment was done with different optics, a different receiver, a different primary calibrator, largely different analysis code, and observed a different part of the sky. Though we have not correlated our data with templates of foreground emission, the foreground contribution is known to be small at these frequencies and galactic latitudes (Coble et al. 1999, de Oliveira-Costa et al. 1997). In addition we have examined the frequency spectrum of the fluctuations in K_a and Q bands, and find it to be consistent with a thermal CMB spectrum, and inconsistent with various foregrounds. Finally, the full analysis has been repeated after deleting each 15° section of data in RA, indicating that the signal does not arise from one region. (Our scan passes near, but misses, the LMC.) Future work will address the precise level of contamination.

We gratefully acknowledge the insights and help from Dave Wilkinson, Norm Jarosik, Ray Blundell, Angel Otárola, Hernán Quintana, Robert Caldwell, Ted Griffith, Bernard Jones, and Harvey Chapman. The experiment would not have been possible without NRAO’s site monitoring and detector development. We also thank Lucent Technologies for donating the radar trailer. This work was supported by an NSF NYI award, a Cottrell Award from the Research Corporation, a David and Lucile Packard Fellowship (to LP), a NASA GSRP fellowship to AM, an NSF graduate fellowship to MN, NSF grants PHY-9222952, PHY-9600015, AST-9732960, and the University of Pennsylvania. The data will be made public upon publication of this *Letter*.

REFERENCES

- Bond, J. R., Efstathiou, G., Lubin, P. M., & Meinhold, P. R. 1991, Phys. Rev. Lett., 66, 2179
- Bond, J. R. 1996 *Theory and Observations of the Cosmic Microwave Background Radiation*, in “Cosmology and Large-Scale Structure,” Les Houches Session LX, August 1993, ed. R. Schaeffer, Elsevier Science Press
- Bond, J. R., Efstathiou, G., & Tegmark, M. 1998, MNRAS, 50, L33
- Bond, J. R., Jaffe, A. H., & Knox, L. 1998, Phys. Rev. D, 57, 2117
- Coble, K., et al. 1999, astro-ph/9902195
- de Oliveira-Costa, A., Kogut, A., Devlin, M. J., Netterfield, C. B., Page, L. A., & Wollack, E. J. 1997 ApJ, 482, L17
- Devlin, M. J., de Oliveira-Costa, A., Herbig, T., Miller, A. D., Netterfield, C. B., Page, L., & Tegmark, M. 1998, ApJ, 509, L73
- Griffith, M. J., Ade, A. R., Orton, G. S., Robson, E. I., Gear, W.K., Nolt, I. G., & Radostitz, J. V. 1986, Icarus, 65, 244
- Hu, W., Sugiyama, N., & Silk, J. 1997, Nature, 386, 37

Jungman, G., Kamionkowski, M., Kosowsky, A., & Spergel, D. N. 1995, Phys. Rev. D, 54, 1332
 Netterfield, C. B., Devlin, M. J., Jarosik, N., Page, L., & Wollack, E. J. 1997, ApJ, 474, 47
 Kerr, A. R., Pan, S.-K., Lichtenberger, A. W., & Lloyd, F. L. 1993, Proceedings of the Fourth International Symposium on Space Terahertz Technology, 1

Pospieszalski, M. W. 1992, IEEE MTT-S Digest, 1369; also see Pospieszalski, M. W. et al. 1994, IEEE MTT-S Digest, 1345
 Pospieszalski, M.W. 1997, Microwave Background Anisotropies (Ed. Frontieres, ed. Bouchet et al.), 23
 Tegmark, M., 1997, Phys. Rev. D, 55, 5895
 Ulich, B. L. 1981, AJ, 86, 1619
 Wollack, E. J., Devlin, M. J., Jarosik, N.J., Netterfield, C. B., Page, L., & Wilkinson, D. 1997, ApJ, 476, 440

TABLE 2
 TOCO97 ANGULAR SPECTRUM

Band/SV	ℓ_{eff}^a	δT_ℓ^b μK	N_{bins}^c	$\delta T'_\ell$ μK	Δ_{tot} μK	Δ_{inst} μK	$\sqrt{I(W)}$	$(A-B)/2^{d,e}$ μK	Quad, q_n^d μK	$(H1-H2)/2^{d,f}$ μK
<i>K_a1/2</i>										
4pt	63^{+17}_{-18}	35^{+13}_{-9}	48(16)	32	33	20	0.84	< 27(0.94)	< 30(1.05)	< 29(0.95)
5pt	86^{+16}_{-21}	52^{+11}_{-8}	64(28)	49	40	21	0.71	< 21(0.59)	< 32(1.23)	< 29(1.05)
6pt	107^{+16}_{-21}	71^{+12}_{-10}	96(42)	69	52	27	0.65	< 32(0.90)	< 31(0.96)	< 35(1.04)
7pt	127^{+16}_{-22}	93^{+15}_{-14}	96(41)	90	57	27	0.55	< 35(0.80)	< 37(0.90)	< 30(0.68)
8pt	145^{+18}_{-20}	103^{+15}_{-13}	128(55)	102	63	34	0.52	< 51(0.97)	< 46(1.00)	< 43(0.91)
9pt	165^{+18}_{-20}	65^{+16}_{-17}	128(54)	59	47	38	0.46	< 63(0.95)	< 72(1.19)	< 66(1.07)
10pt	182^{+21}_{-17}	67^{+20}_{-23}	192(82)	70	60	51	0.44	< 68(0.85)	< 69(0.94)	< 60(0.89)
11pt	192^{+30}_{-8}	< 119	192(82)	67	65	58	0.42	< 91(0.94)	< 83(1.00)	< 86(0.96)
12pt	215^{+27}_{-11}	128^{+30}_{-33}	192(82)	127	83	68	0.37	< 150(1.11)	< 86(0.79)	< 76(0.67)
<i>Q1</i>										
4pt	63^{+17}_{-18}	57^{+18}_{-13}	48(20)	51	53	31	0.83	...	< 44(1.04)	< 47(1.11)
5pt	87^{+16}_{-22}	40^{+14}_{-14}	64(28)	34	40	33	0.71	...	< 36(0.75)	< 47(1.09)
6pt	110^{+15}_{-24}	56^{+14}_{-13}	96(42)	52	52	40	0.65	...	< 45(0.87)	52^{+15}_{-14} (1.71)
7pt	131^{+14}_{-25}	81^{+19}_{-16}	96(42)	77	59	41	0.55	...	< 65(1.12)	< 53(0.89)
8pt	151^{+15}_{-25}	86^{+19}_{-17}	128(55)	79	66	50	0.53	...	< 45(0.67)	< 64(0.89)
9pt	172^{+14}_{-26}	93^{+23}_{-23}	128(55)	89	68	54	0.47	...	< 82(0.94)	< 72(0.83)
10pt	191^{+16}_{-24}	< 115	192(84)	31	75	74	0.47	...	< 105(1.13)	< 92(0.94)
11pt	203^{+17}_{-24}	< 117	192(84)	44	80	78	0.44	...	< 103(0.94)	< 83(0.81)
12pt	221^{+15}_{-15}	< 169	192(84)	91	91	84	0.40	...	< 138(1.06)	< 119(0.92)
13pt	245^{+21}_{-20}	< 130	192(84)	...	84	92	0.37	...	< 163(1.02)	< 164(1.06)
14pt	267^{+20}_{-23}	< 202	256(112)	123	123	114	0.37	...	< 183(1.06)	< 188(1.00)
<i>Q3/4</i>										
5pt	83^{+15}_{-20}	47^{+17}_{-13}	64(17)	43	39	24	0.73	31^{+10}_{-8} (1.94)	< 50(1.39)	< 58(1.73)
6pt	106^{+14}_{-23}	61^{+18}_{-13}	96(22)	55	46	28	0.66	< 27(0.68)	< 34(0.60)	< 61(1.46)
7pt	125^{+14}_{-23}	72^{+16}_{-12}	96(35)	71	50	30	0.56	< 29(0.65)	< 57(1.30)	< 31(0.57)
8pt	145^{+14}_{-23}	115^{+19}_{-15}	128(45)	109	68	35	0.54	< 26(0.50)	< 38(0.73)	< 60(1.18)
9pt	165^{+14}_{-24}	72^{+24}_{-21}	128(29)	65	48	37	0.48	< 43(0.82)	< 97(1.38)	< 84(1.16)
10pt	184^{+15}_{-23}	87^{+19}_{-19}	192(70)	86	63	48	0.47	< 68(1.03)	< 45(0.78)	< 52(0.75)
11pt	196^{+22}_{-17}	90^{+27}_{-26}	192(54)	84	65	53	0.44	< 64(0.90)	< 78(0.91)	< 75(0.78)
12pt	212^{+25}_{-13}	100^{+29}_{-27}	192(65)	97	69	57	0.40	< 70(0.95)	< 129(1.36)	< 84(0.89)
13pt	236^{+20}_{-19}	< 157	192(56)	80	71	65	0.37	< 107(1.07)	< 121(0.93)	< 153(1.17)
14pt	258^{+18}_{-23}	119^{+36}_{-38}	256(103)	119	91	80	0.36	< 116(0.95)	< 137(1.11)	< 103(0.78)

NOTE.—A “<” indicates a 95% confidence limit. Calibration errors are **not** included. (a) The range for ℓ_{eff} denotes the range for which the window function exceeds $e^{-1/2}$ times the peak value. (b) The error on $\delta T_\ell = [\ell(\ell+1)C_\ell/2\pi]^{1/2}$ is comprised of experimental uncertainty and sample variance. These values are not statistically independent: harmonic numbers differing by 2 are correlated at the 0.35 level. For all harmonics, the sample variance ($\propto 1/\sqrt{2N_{\text{bins}}}$) is $\approx 7 \mu\text{K}$. (c) The number of bins on the sky followed by, in parentheses, the number used in the analysis due to the galactic/atmosphere cut. (d) The reduced χ^2 are given in parentheses. (e) $(A-B)/2$ is the difference in polarizations. We have combined bands and harmonics to generate 95% upper limits on polarization, $A-B$, and obtain: $(\ell, \delta T_\ell [\mu\text{K}]) = (63^{+18}_{-18}, < 37)$, $(86^{+17}_{-21}, < 54)$, $(115^{+21}_{-24}, < 28)$, $(148^{+17}_{-25}, < 41)$, $(195^{+33}_{-23}, < 79)$. (f) $(H1-H2)/2$ is the first half minus the second half.

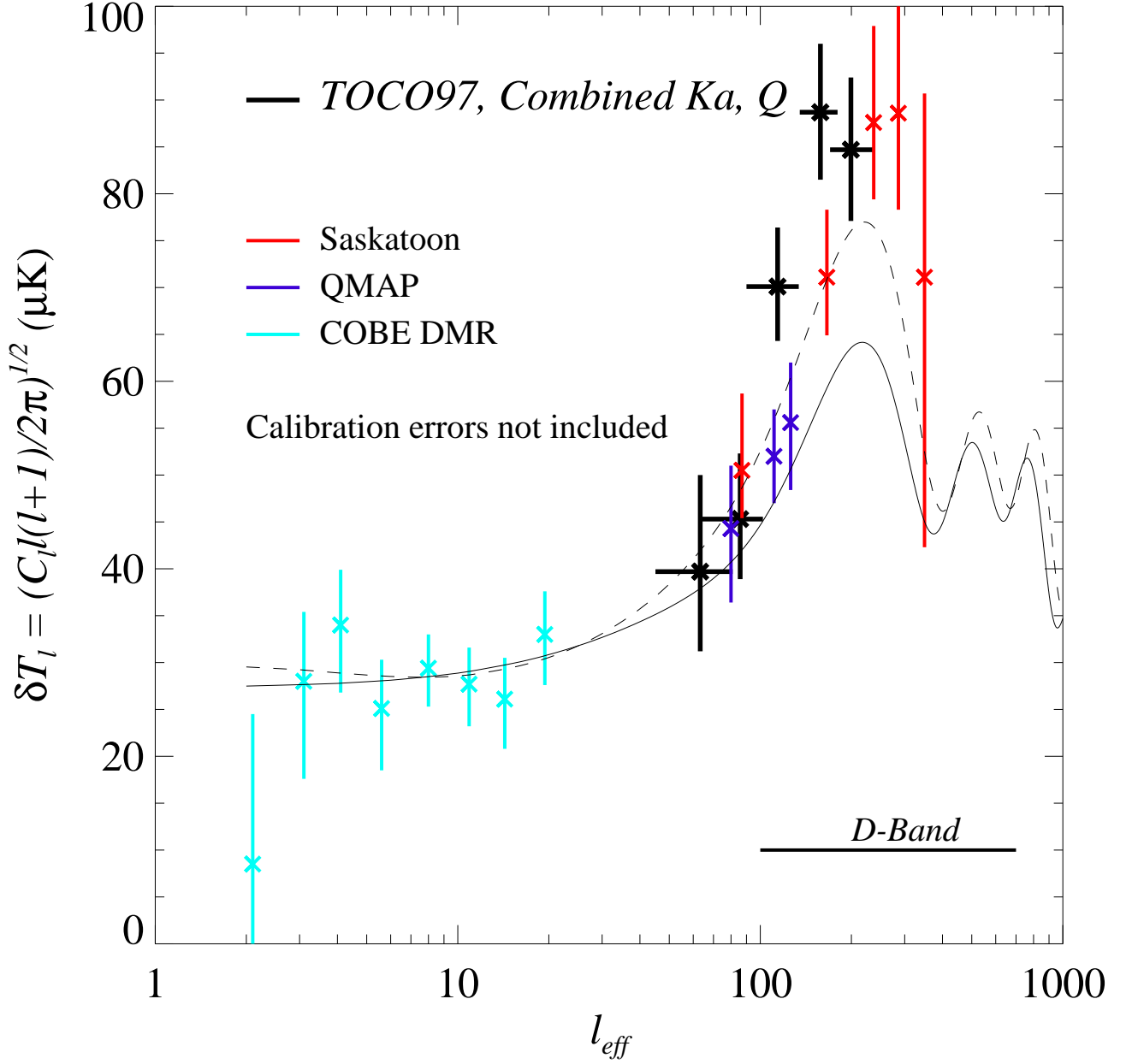


FIG. 3.— Angular spectrum from the SK, QMAP, and TOCO97 experiments. The SK data from Netterfield *et al.* (1997, ApJ, 474:47) and Wollack *et al.* (1997, ApJ 476:440) have been recalibrated according to the Mason *et al.* (1997, astro-ph/9903383), leading to an increase of 5%, and reduced according to the foreground contribution in de Oliveira-Costa *et al.* (1997, ApJL, 482:L17), leading to a reduction of 2%. The foreground reduction was applied uniformly. Because the SK data are primarily at 40 GHz, the Mason *et al.* results must be extrapolated. In addition, uncertainty in the measured passband, measurement uncertainty, and beam uncertainty, must be taken into account. This leads to a 1σ calibration error of 11%. The QMAP data are the same as those reported in de Oliveira-Costa *et al.* (1998, ApJL, 509:L78) and have an average calibration error of 12%, the correction for foreground emission is $\approx 2\%$ (de Oliveira-Costa *et al.* 1999, *in prep*), though has not yet been precisely determined and so is not included. Both SK and QMAP are calibrated with respect to Cas-A. The TOCO97 data, which have a calibration error of 10%, are calibrated with respect to Jupiter. A foreground contribution, which is expected to be small, has not been subtracted. When calibration errors are included, all three independent experiments agree. Two cosmological models are shown for reference. The lower is “standard CDM” ($\Omega_0 = 1$, $\Omega_B = 0.05$, $h = 0.5$); the higher one is the current “concordance model” (Bachall *et al.* 1999 *in prep*, Turner 1999 astro-ph/9904051) with $\Omega_0 = 0.4$, $\Omega_B = 0.045$, $\Omega_\Lambda = 0.6$, and $h = 0.65$. For COBE/DMR we use the results from Tegmark.